



RESEARCH ARTICLE | APRIL 22 2022

Atomic layer etching of Al_2O_3 with NF_3 plasma fluorination and trimethylaluminum ligand exchange

Special Collection: [Atomic Layer Etching \(ALE\)](#)

Jihyun Kim; Dahee Shim; Yongjae Kim; Heeyeop Chae 



J. Vac. Sci. Technol. A 40, 032603 (2022)

<https://doi.org/10.1116/6.0001616>



Articles You May Be Interested In

Thermal atomic layer etching of amorphous and crystalline Al_2O_3 films

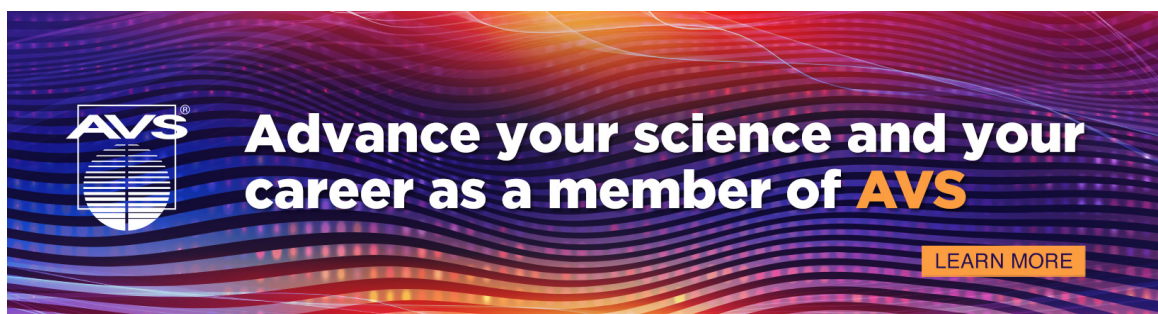
J. Vac. Sci. Technol. A (June 2021)


In situ studies on atomic layer etching of aluminum oxide using sequential reactions with trimethylaluminum and hydrogen fluoride

J. Vac. Sci. Technol. A (April 2022)

Rapid atomic layer etching of Al_2O_3 using sequential exposures of hydrogen fluoride and trimethylaluminum with no purging

J. Vac. Sci. Technol. A (October 2018)





Advance your science and your career as a member of **AVS**

[LEARN MORE](#)

Atomic layer etching of Al_2O_3 with NF_3 plasma fluorination and trimethylaluminum ligand exchange

Cite as: J. Vac. Sci. Technol. A **40**, 032603 (2022); doi: 10.1116/6.0001616

Submitted: 11 November 2021 · Accepted: 4 April 2022 ·

Published Online: 22 April 2022



Jihyun Kim,¹ Dahee Shim,¹ Yongjae Kim,² and Heeyeop Chae^{1,2,a)}

AFFILIATIONS

¹School of Chemical Engineering, Sungkyunkwan University (SKKU), Suwon 16419, Republic of Korea

²SKKU Advanced Institute of Nanotechnology (SAINT), Sungkyunkwan University (SKKU), Suwon 16419, Republic of Korea

Note: This paper is part of the 2023 Special Topic Collection on Atomic Layer Etching (ALE).

a) Author to whom correspondence should be addressed: hchae@skku.edu

ABSTRACT

In this study, a cyclic isotropic plasma atomic layer etching (ALE) process was developed for aluminum oxide that involves fluorination with NF_3 plasma and ligand exchange with trimethylaluminum (TMA). The isotropic plasma ALE consists of two steps: fluorination and removal. During the fluorination step, the Al_2O_3 surface was fluorinated to AlOF_x with NF_3 plasma at 100 °C. The formation of the AlOF_x layer was confirmed by x-ray photoelectron spectroscopy analysis, and the atomic fraction of fluorine on the surface was saturated at 25% after 50 s of plasma fluorination. The depths of the fluorinated layers were in the range of 0.79–1.14 nm at different plasma powers. In the removal step, the fluorinated layer was removed by a ligand exchange reaction with TMA at an elevated temperature range of 250–480 °C. The etch per cycle (EPC) was 0.20–0.30 nm/cycle and saturated after 30 s in the temperature range of 290–330 °C. No etching was observed below 250 °C, and the EPC increased in the temperature range of 250–300 °C during the removal step with the ligand exchange reaction and reached the maximum at 300 °C. Then, the EPC was significantly reduced at high temperatures, possibly due to TMA decomposition. The fluorine atomic fraction on the surface was reduced to 14% after the removal. In conclusion, Al_2O_3 was successfully etched at the atomic scale by the cyclic plasma ALE process. The average surface roughness of Al_2O_3 was reduced from 8.6 to 5.3 Å after 20 cycles of etching.

Published under an exclusive license by the AVS. <https://doi.org/10.1116/6.0001616>

I. INTRODUCTION

Over the last several decades, the critical dimensions (CD) of semiconductor devices have reduced as expressed by Moore's law and recently reached the nanometer scale.^{1–4} The CD reduction has also induced the thickness reduction of gate silicon dioxide for metal-oxide-semiconductor field-effect transistors and a reduction of the lateral dimensions.^{5,6} However, the continuous decrease in SiO_2 thickness, approaching the permissible limits, has led to large gate leakage currents.^{5,7–9} High-dielectric constant (κ) materials have been adopted to replace SiO_2 to enable the thickness reduction by blocking the leakage current at the limited thickness.^{6,7,10,11} High- κ materials, such as Al_2O_3 , ZrO_2 , and HfO_2 , provide the specific capacitance required for the gate dielectric at a considerable thickness with a reduced leakage current of transistors.^{10,12,13} Among them, Al_2O_3 is

considered a potential candidate for the blocking oxides in charge-trap flash memory applications owing to its larger bandgap (7 eV) than other high- κ materials, such as ZrO_2 (4.6 eV) and HfO_2 (5.7 eV).^{14,15} However, Al_2O_3 is difficult to etch because of its physical and chemical stabilities and is typically etched by reactive ion etching (RIE).^{16–18} The use of three-dimensional (3D) structures is another miniaturization solution that requires a different etching technology than the conventional methods.⁴ The RIE results in anisotropic patterns and, therefore, cannot be applied to make 3D structures that require isotropic etching.^{4,19,20} Isotropic atomic layer etching (ALE) technologies are required to fabricate 3D structures with atomic scale dimensions.^{20–24}

Isotropic ALE for Al_2O_3 is typically carried out by the surface fluorination and removal reactions, which are separated by purge steps.^{22,25–29} The fluorination is typically the first modification step

18 July 2025 11:52:17

that converts the surface of Al_2O_3 to AlF_3 using hydrogen fluoride at elevated substrate temperatures.^{25,26,30–32} Al_2O_3 at the surface is converted into an AlF_3 layer by reacting with HF because AlF_3 is more thermodynamically stable and reactive than Al_2O_3 .^{4,25,26} However, the use of HF should be restricted owing to safety issues related to its highly corrosive nature.³⁰ Fluorine-containing plasma processing can be an alternative method to replace HF for the fluorination of surfaces.^{22,25,30} The high reactivity of plasma can broaden the choice of the fluorinating agent for isotropic ALE.^{21,22} The second stage of isotropic ALE comprises the removal step using thermal reactions, such as ligand exchange reactions, to remove the fluorinated surface.^{29,30,35–35} The isotropic plasma ALE for Al_2O_3 has been previously studied, but not as much as thermal ALE.^{22,36} A previous ALE study using plasma was characterized by etch rate and etch profiles.²² However, the study on fluorination on the surface and that in different depths using plasma fluorination has not been reported yet.

In this study, a cyclic isotropic plasma ALE process was developed for Al_2O_3 by employing NF_3 , inductively coupled plasma (ICP), and trimethylaluminum (TMA) ligand exchange. The Al_2O_3 surface was fluorinated to AlOF_x with NF_3 plasma in the fluorination step, and the fluorinated layer was removed by a ligand exchange process with TMA at elevated temperatures in the removal step. The depth of the fluorinated layer was analyzed for different radio frequency (RF) powers in the fluorination step and etched. Surface analysis was performed after each half cycle. The etch per cycle (EPC), which was dependent on the exposure time of TMA, was saturated at various temperatures. The surface roughness of Al_2O_3 decreased after the cyclic isotropic plasma ALE process.

II. EXPERIMENT

A cyclic isotropic plasma ALE was studied in an ICP reactor with halogen lamps surrounding the quartz tube, as shown in Fig. 1(a). RF power was supplied through an inductive coil at 13.56 MHz to generate plasma. Six halogen lamps were used for heating the sample to 480 °C. Al_2O_3 films that are 50 nm-thick were prepared on a silicon substrate by physical vapor deposition sputtering to study the isotropic plasma ALE. Al_2O_3 test samples of dimensions $1.5 \times 1.5 \text{ cm}^2$ were positioned on $5 \times 5 \text{ cm}^2$ Si carrier wafers and placed at the center of the heating lamp.

The isotropic plasma ALE process sequence for Al_2O_3 is shown in Fig. 1(b). One cycle is composed of two steps: fluorination and removal. The first step in surface fluorination is the conversion reaction of the Al_2O_3 layer to the AlOF_x layer using plasma at 100 °C. The temperature of the fluorination step was maintained at 100 °C for 60 s, and the halogen lamps were turned on to elevate the temperature by 300 °C for 30 s after the fluorination in the first purge step. NF_3 , at a mass flow rate of 3.0 SCCM was exposed to surface fluorination, and the pressure was maintained at 35 mTorr. The applied RF power source was operated at 10 W for 60 s. The second step, AlOF_x layer removal, was achieved by a ligand exchange reaction with TMA at elevated temperatures. The temperature was increased to 300 °C by turning the halogen lamps and the temperature was maintained for 30 s with 50 SCCM TMA and 50 SCCM Ar. After this removal step, the sample was cooled for 180 s in the following purge step before the

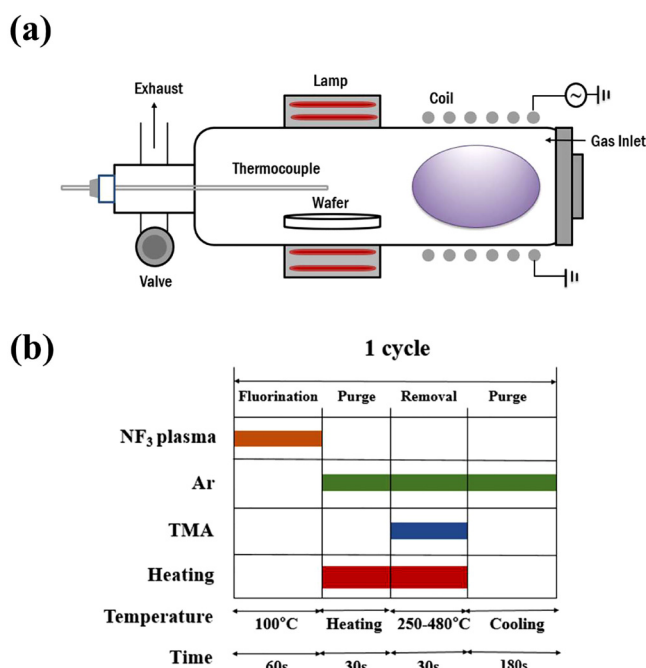


FIG. 1. (a) Schematic of ICP-type PECVD reactor and (b) sequence of the isotropic plasma ALE process for Al_2O_3 etching.

temperature reaches 100 °C. These two sequential steps were repeated to etch the Al_2O_3 layer.

The thickness of the fluorinated layer was measured using secondary ion mass spectrometry (SIMS, IONTOF, TOF-SIMS-5) after the fluorination step. Cs^+ (1 keV, 40 nA) was used to remove the material forming a $150 \times 150 \mu\text{m}^2$ sputter crater, and Bi^+ ion (25 keV, 1 pA) was used for elemental analysis. The etch rate of the Al_2O_3 layer was measured by changing the thickness of the removed Al_2O_3 layer using a spectroscopic ellipsometer (Ellipso-Technology, Elli-SE-U) before and after the process. X-ray photoelectron spectroscopy (XPS, Thermo Scientific, ESCALAB 250) was used to characterize the chemical bonding structure and surface atomic composition of the Al_2O_3 surface. High-resolution atomic force microscopy (HR-AFM, JPK Instruments, Nano Wizard Ultra Speed) was used to confirm the surface roughness after etching.

III. RESULTS AND DISCUSSION

As the first step, Al_2O_3 was fluorinated with NF_3 plasma, and the surface was analyzed by varying the plasma RF power and processing time. The depths of the fluorinated layers were investigated by SIMS depth profiling at various RF powers, as shown in Fig. 2(a). The F peak increased significantly with the RF power due to highly reactive fluorine radicals generated in the plasma. The fluorinated depth is defined as the depth at which the F intensity drops to 80% of its maximum intensity.³⁷ The fluorination thickness is not saturated with the RF power, and the increase in the depth of fluorination is attributed to an increase in fluorine radicals generated at high

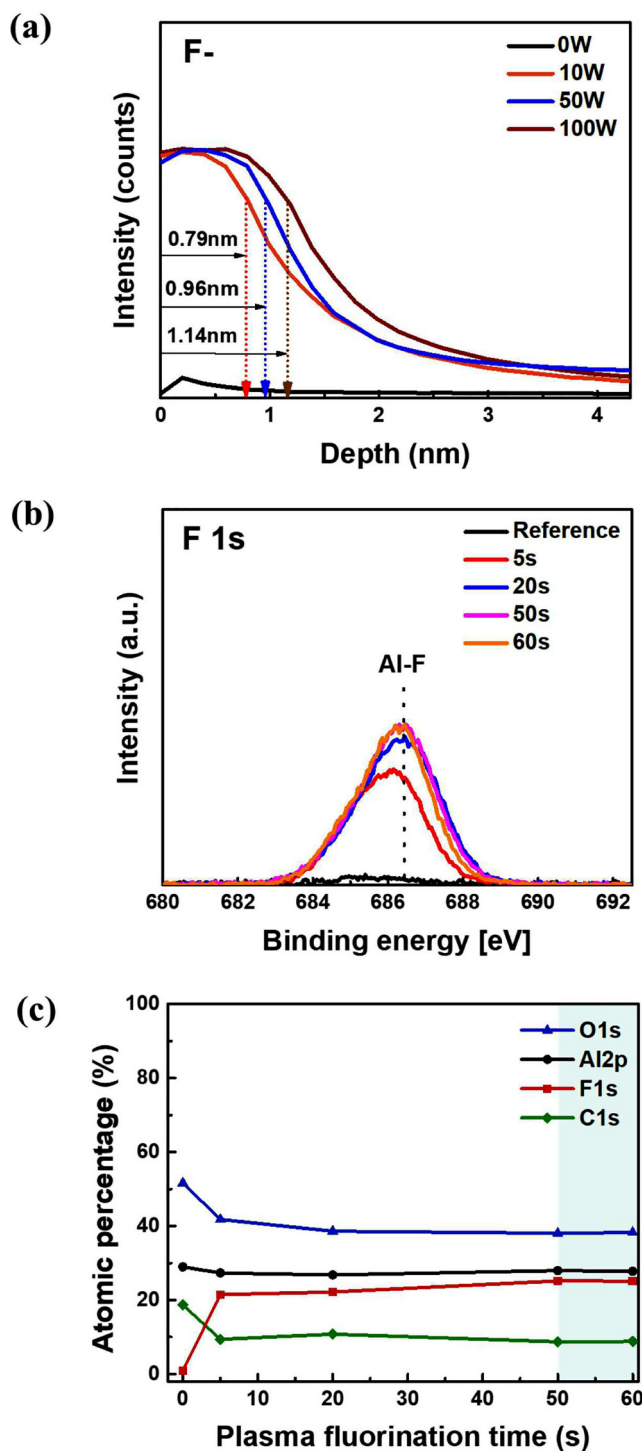


FIG. 2. (a) SIMS depth profiles of F as a function of the sputtering time after NF_3 plasma treatment for 60 s at 0, 10, 50, and 100 W; (b) F 1s XPS peak from Al_2O_3 films; and (c) saturation of atomic fractions as NF_3 plasma exposure time at 10 W and 100 °C.

RF powers.^{38,39} A similar phenomenon is observed in the plasma oxidation of silicon. The oxidation thickness increased by plasma power without saturation.^{34,40} The fluorination as a function of NF_3 plasma processing time was investigated with the F1s peak at the binding energy of 686.3 eV in the XPS spectra, as shown in Fig. 2(b).⁴¹ The peak increases with NF_3 plasma time up to 50 s and thereafter saturates at an RF power of 10 W. The F1s peak is saturated because the fluorinated layer acts as a diffusion barrier that prevents fluorine from further penetrating the Al_2O_3 layer.²² The atomic surface compositions of Al, O, and F were also plotted as a function of the fluorination time, as shown in Fig. 2(c). The atomic fraction of F increased to 25% and that of O decreased from 38% to 51% after 50 s of NF_3 plasma. The decrease in O is caused by the removal of NO or NO_2 in the NF_3 plasma.³⁵ All the atomic compositions were saturated after 50 s of NF_3 plasma exposure time, and therefore, the plasma time of 60 s was selected as the standard time for the following fluorination step. The saturation in the fluorination step with NF_3 plasma allows precise control of the etch rate in the ALE process.

As the next step, the chemical composition of the fluorinated layer processed under the 60 s and 10 W conditions was investigated using XPS and SIMS depth profiles, as shown in Fig. 3. Al 2p peak was analyzed for fluorination, and the peak was deconvoluted into three peaks of 74.5, 75.8, and 76.5 eV, representing Al_2O_3 , AlOF_x , and AlF_3 , respectively, as shown in Fig. 3(a).⁴² The peak area fractions of AlOF_x and AlF_3 correspond to ~56.7% and ~7.6%, respectively, of the total area. The depth profiles of O, F, Al, AlO, and AlOF were analyzed by SIMS at different sputtering times, as shown in Fig. 3(b). High concentrations of F and AlOF were observed near the surface region, indicating a high degree of fluorination on the surface. The intensity of F increased slightly near the surface and decreased significantly with depth. The low O and AlO fractions near the surface are attributed to the replacement of O by F in the fluorination step.⁴³

The fluorinated Al_2O_3 and AlOF_x were removed by a ligand exchange reaction with TMA in the next step, and the EPC was studied as a function of the temperature and TMA exposure time as shown in Fig. 4(a). The EPC plateaus after 30 s of TMA exposure at various temperatures, and, therefore, 30 s was selected as the standard TMA exposure time in the subsequent study on the removal step. TMA exposure time in this work is considerably longer than that of HF in previous studies.^{21,35,44–46} We believe that this longer TMA exposure time is attributed to a thicker fluorination depth formed with reactive fluorine radicals. The EPC increased from 0.20 to 0.30 nm/cycle when the temperature was increased from 290 to 300 °C and decreased to 0.27 nm/cycle at 330 °C. The EPC at 300 °C in this work is approximately 2–7 times higher with plasma fluorination than that with HF.^{21,35,44–46} The saturated EPC at 30 s of TMA processing was plotted over the entire temperature range, as shown in Fig. 4(b). No etching was observed below 250 °C, and the EPC increases at the temperature range of 250–300 °C. The EPC sharply decreases above 300 °C, and no etching was observed above 480 °C. We analyzed the surface composition with XPS at higher temperature of 280–480 °C as shown in Fig. 4(c). C1s peaks were fit using C–C at 284.5 eV and C–F_x (x = 1, 2, 3) at 288.7 eV.^{47,48} The C1s peaks maintained the similar intensity with and without TMA in the temperature range of 280–300 °C after first cycle ALE process. The intensities of C–C

18 JULY 2025 11:52:17

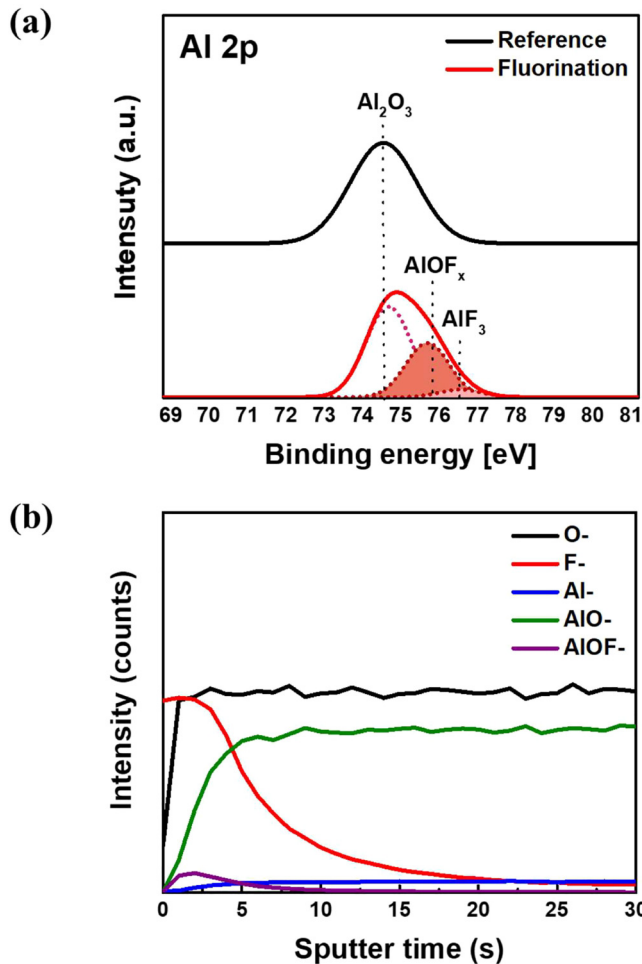


FIG. 3. (a) Al 2p XPS peak and (b) SIMS depth profiles of O, F, Al, AlO, and AlOF of Al_2O_3 surface after 60 s exposures using NF_3 at 10 W and 100 °C.

and C-F_x peaks increase at the temperature above 300 °C, and the increase of carbon on the surface is believed to be related to the decomposition of TMA at higher temperature. The monomers of TMA were reported to decompose into dimethyl aluminum, monomethyl aluminum, C_2H_4 , and CH_3 at high temperatures in a previous study.⁴⁹ The decrease of EPC is attributed to the increased carbon on surface at higher temperature above 300 °C.

The etched depth after each ALE cycle was compared with the depth of the fluorinated layer at RF powers of 10, 50, and 100 W via SIMS depth profiling, as shown in Fig. 5(a). Both the fluorinated depth and etched depth increased with the increasing RF power. However, the etched depth was less than the fluorinated depth, indicating that the fluorinated layers were not completely removed from the surface after the ALE. The ratio of fluorinated layer depth to etched depth was almost constant at 2.6 at each RF power. The atomic compositions of the Al_2O_3 surface were analyzed at 10 W by XPS and are plotted in Fig. 5(b) after each fluorination and removal

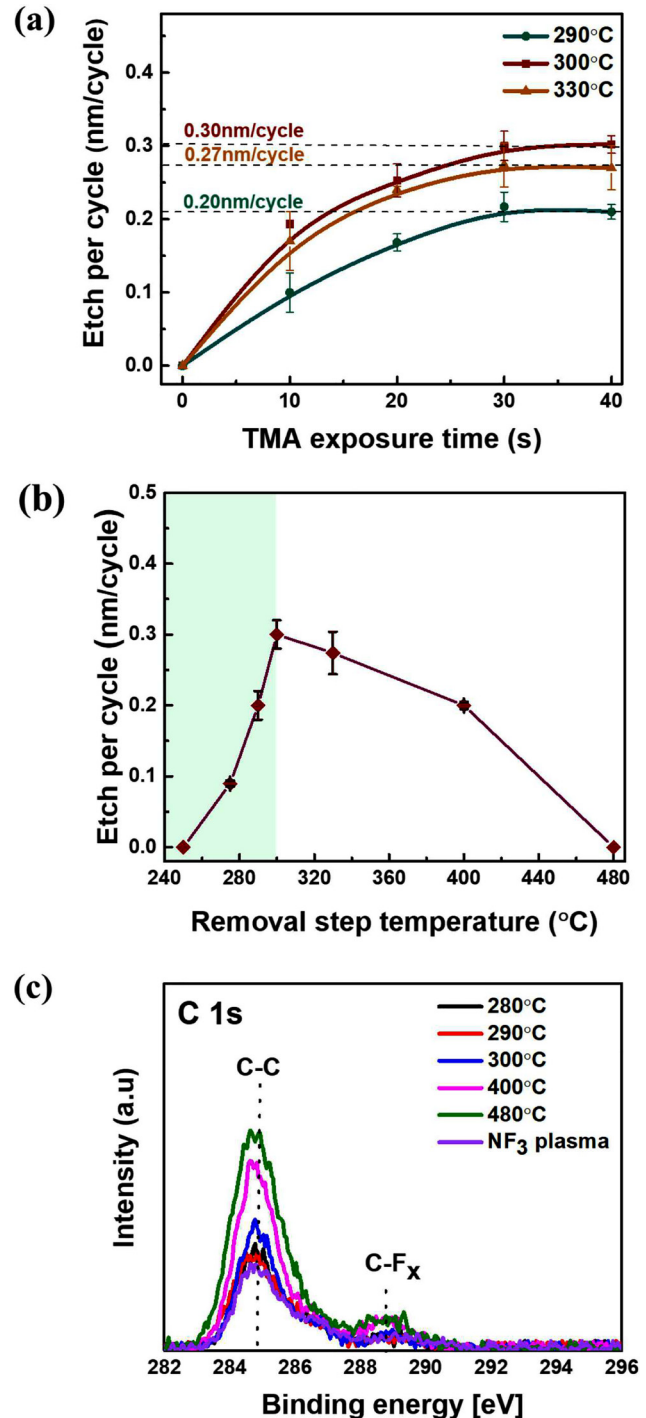


FIG. 4. (a) TMA exposure time at 290, 300, and 330 °C of the removal step; (b) EPC using $\text{NF}_3/\text{TMA} = 60/30$ s at the range of 250–480 °C of the removal step; and (c) C 1s XPS peak from Al_2O_3 films after NF_3 plasma exposure time at 10 W and 100 °C and after removal step at an elevated temperature range of 280–480 °C.

18 July 2025 11:52:17

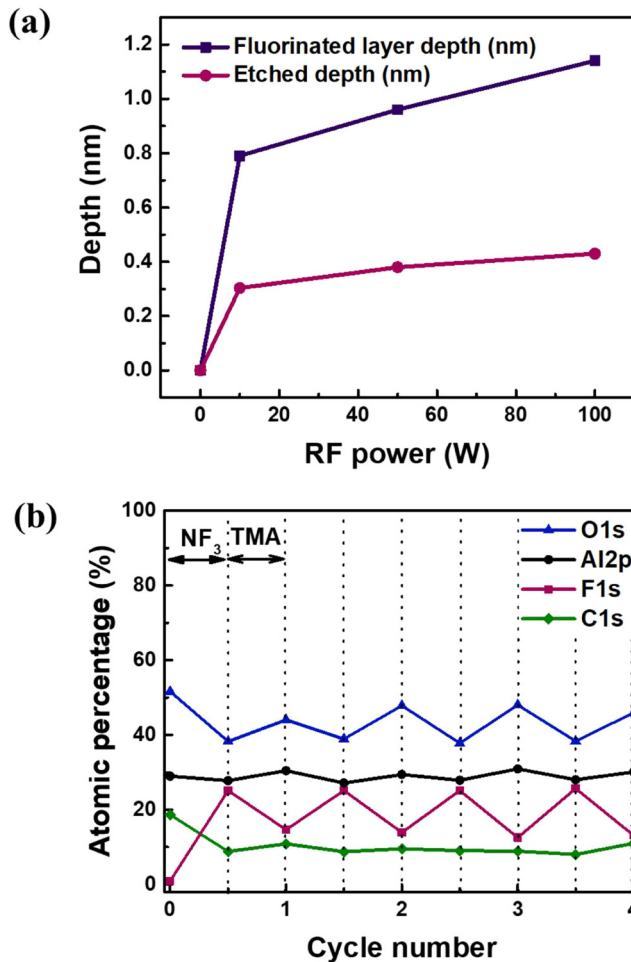


FIG. 5. (a) Depth comparison of each half cycle of the fluorination step for 60 s NF_3 plasma at 10, 50, and 100 W and a temperature of 100 °C, and the removal step with TMA for 30 s at an elevated temperature of 300 °C and (b) surface atomic fraction tendency at each half cycle at 10 W.

step. The concentration of fluorine was increased by 25% owing to the formation of AlOF_x layers on Al_2O_3 with NF_3 plasma in the first fluorination step. The fluorine concentration of the surface dropped to 14% after the reaction with TMA during the first removal step. The concentration of fluorine increased to 25% after the second fluorination step and decreased to 14% after the second removal step. In conclusion, this ALE process removes Al_2O_3 at the atomic scale, even though the process leaves a fluorine residue on the surface after the plasma ALE process.

The surface roughness of the Al_2O_3 films were observed by HR-AFM to image and quantify the roughness after the isotropic plasma ALE process, as shown in Fig. 6. As the number of cycles increased, the surface morphology became smooth, as shown in Fig. 6(a). The average roughness of the initial Al_2O_3 surface was 8.6 Å and increased to 26.6 Å after first fluorination step possibly

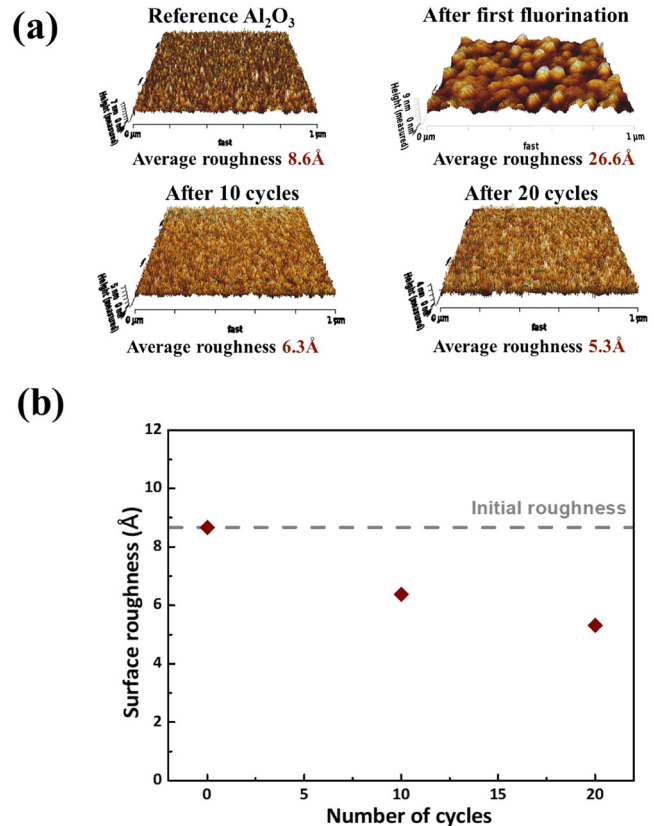


FIG. 6. (a) Surface morphology and (b) reduction of surface roughness after isotropic ALE process as a function of the number of cycles.

due to reorganization into AlOF_x layer.^{25,50} The lower surface roughness was achieved by a chemical reaction between the fluorinated layer and TMA during the ligand exchange reaction. The average roughness of Al_2O_3 decreases significantly by 5.3 Å after a 20-cycle process as shown in Fig. 6(b). From the literature, the surface roughness, determined after a thermal ALE process using HF via x-ray reflectivity, decreased from 6.26 to 3.56 Å after 100 cycles of ALE process at 300 °C.⁴⁶ This study using plasma for ALE effectively lowers the surface roughness as smoothly as the thermal ALE within only 20 cycles.

IV. SUMMARY AND CONCLUSIONS

A plasma NF_3 ALE process for Al_2O_3 was developed in this study. The depth of the fluorinated layer was confirmed to be 0.79 nm using NF_3 plasma at 10 W. The Al_2O_3 surface was fluorinated to AlOF_x with NF_3 plasma, and all atomic fractions of this surface were saturated as a function of the NF_3 plasma processing time at a fluorine concentration of 25%. The self-limiting characteristics were confirmed at various temperatures and TMA exposure times, and an EPC of 0.30 nm/cycle was achieved at a temperature of 300 °C. After the ALE process, the fluorine concentration of

18 July 2025 11:52:17

the surface dropped to 14% after the reaction with TMA. The etched depth at 10 W increased with the increasing RF power and the plasma ALE process demonstrated atomic scale etching even though the surface remained fluorinated. The roughness of the Al₂O₃ substrate was decreased from 8.6 to 5.3 Å after a 20-cycle ALE process. We demonstrated that the proposed process with the use of plasma is an effective and nondestructive technique for the atomic level etching of 3D structures.

ACKNOWLEDGMENTS

This work was supported by the National Research Foundation of Korea (NRF) grant funded by the Korea Government (MSIT) (No. 2018R1A2A3074950) and by the Korea Institute for Advancement of Technology (KIAT) and the Ministry of Trade, Industry & Energy (MOTIE) of the Republic of Korea (No. P0017363).

AUTHOR DECLARATIONS

Conflict of Interest

The authors have no conflicts to disclose.

DATA AVAILABILITY

The data that support the findings of this study are available from the corresponding author upon reasonable request.

REFERENCES

- ¹Y.-T. Oh, K.-B. Kim, S.-H. Shin, H. Sim, N. Van Toan, T. Ono, and Y.-H. Song, *Microelectron. Eng.* **79**, 1 (2018).
- ²J. U. Knickerbocker *et al.*, 2008 58th Electronic Components and Technology Conference, Lake Buena Vista, FL, 27–30 May 2008 (2008).
- ³S. Ye, K. Yamabe, and T. Endoh, *Mater. Sci. Semicond. Process.* **134**, 106046 (2021).
- ⁴A. Fischer, A. Routzahn, S. M. George, and T. Lill, *J. Vac. Sci. Technol. A* **39**, 030801 (2021).
- ⁵M. Hirose, M. Koh, W. Mizubayashi, H. Murakami, K. Shibahara, and S. Miyazaki, *Semicond. Sci. Technol.* **15**, 485 (2000).
- ⁶D. Rathee, M. Kumar, and S. K. Arya, *Int. J. Comput. Appl.* **8**, 10 (2010).
- ⁷R. Chau, S. Datta, M. Doczy, J. Kavalieros, and M. Metz, Extended Abstracts of International Workshop on Gate Insulator (IEEE Cat. No. 03EX765), Tokyo, Japan, 6–7 November 2003 (2003).
- ⁸S. Saha, *J. Vac. Sci. Technol. B* **19**, 2240 (2001).
- ⁹Q. Chen and J. D. Meindl, *Nanotechnology* **15**, S549 (2004).
- ¹⁰J. A. Kittl *et al.*, *Microelectron. Eng.* **86**, 1789 (2009).
- ¹¹C. Zhao, C. Zhao, S. Taylor, and P. Chalker, *Materials* **7**, 5117 (2014).
- ¹²K. Takahashi, K. Ono, and Y. Setsuhara, *J. Vac. Sci. Technol. A* **23**, 1691 (2005).
- ¹³K. Yim, Y. Yong, J. Lee, K. Lee, H.-H. Nahm, J. Yoo, C. Lee, C. Seong Hwang, and S. Han, *NPG Asia Mater.* **7**, e190 (2015).
- ¹⁴X. Yang, J.-C. Woo, D.-S. Um, and C.-I. Kim, *Trans. Electr. Electron. Mater.* **11**, 202 (2010).
- ¹⁵W. Ban, S. Kwon, J. Nam, J. Yang, S. Jang, and D. Jung, *Thin Solid Films* **641**, 47 (2017).
- ¹⁶D.-P. Kim, J.-W. Yeo, and C.-I. Kim, *Thin Solid Films* **459**, 122 (2004).
- ¹⁷J. Paul *et al.*, *Microelectron. Eng.* **86**, 949 (2009).
- ¹⁸D. W. Kim, C. H. Jeong, K. N. Kim, H. Y. Lee, H. S. Kim, Y. J. Sung, and G. Y. Yeom, *Thin Solid Films* **435**, 242 (2003).
- ¹⁹K. S. Min, S. H. Kang, J. K. Kim, Y. I. Jhon, M. S. Jhon, and G. Y. Yeom, *Microelectron. Eng.* **110**, 457 (2013).
- ²⁰A. Fischer, A. Routzahn, and T. Lill, ECS Meeting Abstracts **MA2020-02** (2020).
- ²¹Y. Lee, J. W. DuMont, and S. M. George, *Chem. Mater.* **28**, 2994 (2016).
- ²²N. J. Chittock, M. F. J. Vos, T. Faraz, W. M. M. Kessels, H. C. M. Knoops, and A. J. M. Mackus, *Appl. Phys. Lett.* **117**, 162107 (2020).
- ²³N. Miyoshi, H. Kobayashi, K. Shinoda, M. Kurihara, T. Watanabe, Y. Kouzuma, K. Yokogawa, S. Sakai, and M. Izawa, *Jpn. J. Appl. Phys.* **56**, 06HB01 (2017).
- ²⁴W. Lu, Y. Lee, J. C. Gertsch, J. A. Murdzek, A. S. Cavanagh, L. Kong, J. A. Del Alamo, and S. M. George, *Nano Lett.* **19**, 5159 (2019).
- ²⁵V. Sharma, S. D. Elliott, T. Blomberg, S. Haukka, M. E. Givens, M. Tuominen, and M. Ritala, *Chem. Mater.* **33**, 2883 (2021).
- ²⁶S. M. George, *Acc. Chem. Res.* **53**, 1151 (2020).
- ²⁷J. W. DuMont and S. M. George, *J. Chem. Phys.* **146**, 052819 (2017).
- ²⁸Y. Kim, S. Lee, Y. Cho, S. Kim, and H. Chae, *J. Vac. Sci. Technol. A* **38**, 022606 (2020).
- ²⁹Y. Cho, Y. Kim, S. Kim, and H. Chae, *J. Vac. Sci. Technol. A* **38**, 022604 (2020).
- ³⁰J. C. Gertsch, A. M. Cano, V. M. Bright, and S. M. George, *Chem. Mater.* **31**, 3624 (2019).
- ³¹C. Fang, Y. Cao, D. Wu, and A. Li, *Prog. Nat. Sci. Mater. Int.* **28**, 667 (2018).
- ³²J. W. Clancey, A. S. Cavanagh, J. E. T. Smith, S. Sharma, and S. M. George, *J. Phys. Chem. C* **124**, 287 (2020).
- ³³J. A. Murdzek, A. Rajashekhar, R. S. Makala, and S. M. George, *J. Vac. Sci. Technol. A* **39**, 042602 (2021).
- ³⁴A. M. Cano, A. E. Marquardt, J. W. DuMont, and S. M. George, *J. Phys. Chem. C* **123**, 10346 (2019).
- ³⁵S. M. George and Y. Lee, *ACS Nano* **10**, 4889 (2016).
- ³⁶A. Fischer, R. Janek, J. Boniface, T. Lill, K. Kanarik, Y. Pan, V. Vahedi, and R. A. Gottscho, *Proc. SPIE* **10149**, 101490H (2017).
- ³⁷Z. Wang, C. Carrière, A. Seyeux, S. Zanna, D. Mercier, and P. Marcus, *J. Electrochem. Soc.* **168**, 041503 (2021).
- ³⁸Y.-F. Wang, L.-C. Wang, M. Shih, and C.-H. Tsai, *Chemosphere* **57**, 1157 (2004).
- ³⁹G. Bruno, P. Capezzuto, G. Cicala, and P. Manodoro, *J. Vac. Sci. Technol. A* **12**, 690 (1994).
- ⁴⁰Y. Huang *et al.*, *Sol. Energy Mater. Sol. Cells* **208**, 110389 (2020).
- ⁴¹S. W. King, R. F. Davis, and R. J. Nemanich, *J. Vac. Sci. Technol. A* **32**, 051402 (2014).
- ⁴²R. Ramos, G. Cunge, B. Pelissier, and O. Joubert, *Plasma Sources Sci. Technol.* **16**, 711 (2007).
- ⁴³C. S. Lai, K. M. Fan, H. K. Peng, S. J. Lin, C. Y. Lee, and C. F. Ai, *Appl. Phys. Lett.* **90**, 172904 (2007).
- ⁴⁴Y. Lee, C. Huffman, and S. M. George, *Chem. Mater.* **28**, 7657 (2016).
- ⁴⁵J. Hennessy, C. S. Moore, K. Balasubramanian, A. D. Jewell, K. France, and S. Nikzad, *J. Vac. Sci. Technol. A* **35**, 041512 (2017).
- ⁴⁶D. R. Zywotko, J. Faguet, and S. M. George, *J. Vac. Sci. Technol. A* **36**, 061508 (2018).
- ⁴⁷S.-K. Kang, J. S. Oh, B. J. Park, S. W. Kim, J. T. Lim, G. Y. Yeom, C. J. Kang, and G. J. Min, *Appl. Phys. Lett.* **93**, 043126 (2008).
- ⁴⁸J. Chastain and R. C. King, Jr., *Handbook of X-ray photoelectron spectroscopy* (Perkin-Elmer, 1992), p. 261.
- ⁴⁹Z. Zhang, Y. Pan, J. Yang, Z. Jiang, and H. Fang, *J. Cryst. Growth* **473**, 6 (2017).
- ⁵⁰K. Miwa, K. Usami, N. Takada, and K. Sasaki, *Jpn. J. Appl. Phys.* **48**, 126002 (2009).

18 July 2025 11:52:17